

# Optimization of multilayer antireflection coatings on the front surface of N-type TOPCon solar cells

MEILING ZHANG<sup>1</sup>, MEILIN PENG<sup>1</sup>, QIQI WANG<sup>1</sup>, XI XI<sup>1,2\*</sup>, GUILIN LIU<sup>1,2</sup>, JIANBO SHAO<sup>1</sup>

<sup>1</sup>School of Science, Jiangnan University, Wuxi, 214122, China

<sup>2</sup>Jiangsu Provincial Research Center of Light Industrial Optoelectronic Engineering and Technology, Wuxi 214122, China

The application of antireflection film can reduce the Fresnel reflection at the gas-solid interface, representing an effective method of improving the power conversion efficiency of crystalline silicon solar cells. The N-type Tunnel Oxide Passivated Contact (TOPCon) solar cells typically employ  $\text{AlO}_x/\text{SiN}_x$  as the antireflection film, but the thickness adjustment range of the  $\text{AlO}_x$  layer is limited by the passivation effect, so the adjustment of the antireflection effect depends more on the  $\text{SiN}_x$  layer. In this paper, to solve the problem of refractive index matching, the  $\text{SiN}_x/\text{SiO}_x$  and  $\text{SiN}_x/\text{SiO}_x\text{N}_y/\text{SiO}_x$  antireflection stacks were proposed. Compared with the  $\text{SiN}_x$  monolayer,  $\text{SiN}_x/\text{SiO}_x$  and  $\text{SiN}_x/\text{SiO}_x\text{N}_y/\text{SiO}_x$  stacks can significantly reduce the photon reflectivity in the wavelength range of 300-500 nm, and the antireflection effect was better in the short wavelengths. Compared with the electrical performances of traditional solar cells only with  $\text{SiN}_x$  layer, the power conversion efficiency of the cells with  $\text{SiN}_x/\text{SiO}_x$  stack reached 24.68%, and the cells with  $\text{SiN}_x/\text{SiO}_x\text{N}_y/\text{SiO}_x$  stack reached 24.78%, which was 0.2%<sub>abs.</sub> and 0.3%<sub>abs.</sub> higher than the former respectively. The film thickness of the  $\text{SiN}_x/\text{SiO}_x\text{N}_y/\text{SiO}_x$  stack layer was further optimized, ultimately determining that the thickness of  $\text{SiN}_x/\text{SiO}_x\text{N}_y/\text{SiO}_x$  was 60 nm/10 nm/15 nm, respectively. The optimum thickness combination of the antireflective coating in this study provides insights into achieving a conversion efficiency of 24.84% for TOPCon solar cells.

(Received July 24, 2024; accepted April 15, 2025)

**Keywords:** TOPCon solar cells, Antireflection coating, Optical reflectivity, Transmitted photon flux density

## 1. Introduction

As an essential support for the global energy transition, the photovoltaic (PV) industry has developed rapidly in recent years. Crystalline silicon solar cells have become the most widely used PV devices in the market due to their low cost and high-power conversion efficiency [1]. In 2013, the Fraunhofer-ISE Institute of Germany proposed Tunnel Oxide Passivated Contact (TOPCon) solar cells [2,3]. An ultra-thin oxide layer ( $\text{SiO}_x$ ) and a heavily doped polycrystalline silicon (poly-Si) layer were introduced as the rear passivation stack. This structure effectively inhibits the passage of minority carriers while promoting the tunneling of majority carriers, thus reducing the recombination of carriers and improving the power conversion efficiency of the solar cells. Due to its excellent passivation and carrier transportation structural characteristics, TOPCon solar cells have become a hotspot of crystalline silicon solar cells.

The antireflection coating (ARC) of solar cells effectively improves the effective utilization of photons, so the deposition of ARC is an effective way to improve the power conversion efficiency of solar cells [4]. The antireflection layer reduced the reflectivity of sunlight on the silicon wafer surface based on the thin-film interference principle. The optical reflectivity of bare silicon surface is higher than 30%, while it can be reduced to approximately

10% by depositing a film with appropriate thickness and refractive index [5-7]. For traditional P-type crystalline silicon solar cells, the front ARC was a single  $\text{SiN}_x$  layer deposited by plasma-enhanced chemical vapor deposition (PECVD) equipment [8-10]. TOPCon solar cells use an N-type silicon substrate with a higher minority lifetime than a P-type silicon substrate. For the TOPCon solar cell, the front emitter surface was P-type, and it is not suitable to use a positively charged  $\text{SiN}_x$  film as a passivation layer [11,12]. Therefore, the use of laminated films was widely used in the production of solar cells, such as  $\text{SiO}_x\text{N}_y/\text{SiO}_x$ ,  $\text{SiN}_x/\text{SiO}_x\text{N}_y/\text{SiO}_x$  films. The laminated film not only has low reflectivity, but also high durability [13-16].  $\text{SiN}_x$  is a semiconductor material with excellent physical and chemical properties due to its high dielectric constant and corrosion resistance [17,18]. However, the extinction coefficient of  $\text{SiN}_x$  films increases significantly with the increase of refractive index [17].  $\text{SiN}_x$  films have a high light absorption below the wavelength of 500 nm, which influences the photon absorption inside the Si wafer and reduces the photon-generation carriers, as well as the short circuit current of the solar cell, resulting in a decrease in efficiency [19]. Meanwhile, the refractive index of  $\text{AlO}_x$  layer is lower than that of  $\text{SiN}_x$  layer. This prevents the refractive index of the dielectric layer through which light passes from increasing sequentially, which has a certain impact on the antireflection effect.

In addition, to ensure the passivation effect, the thickness adjustment range of the  $\text{AlO}_x$  layer is greatly limited, thus, the adjustment of antireflection is more dependent on the  $\text{SiN}_x$  layer. Therefore, the front antireflection impact of the cell has also become one of the essential factors affecting the conversion efficiency of TOPCon solar cells. To solve these problems, this paper considered adding other materials to prepare multilayer antireflection coating structures.

Due to its low refractive index, high hardness and strong protective force,  $\text{SiO}_x$  is an excellent material for the preparation of optical antireflection coatings [20,21]. At the same time, the refractive index matching between each layer is also very important. The larger the refractive index difference between the adjacent layers, the larger of the optical reflectivity is. Therefore, it is vital to introduce  $\text{SiO}_x\text{N}_y$  as a refractive index transition layer. The refractive index of  $\text{SiO}_x\text{N}_y$  ( $n_2=1.85$ ) prepared by PECVD is between  $\text{SiO}_x$  ( $n_1=1.55$ ) and  $\text{SiN}_x$  ( $n_3=2.05$ ), which allows an excellent refractive index matching of the multilayer films. Moreover,  $\text{SiO}_x\text{N}_y$  has high hardness, high-temperature stability, and high-temperature oxidation resistance [22], which is very suitable for forming multilayer structures with  $\text{SiN}_x$ .

Based on the above theories, in this study, the traditional  $\text{AlO}_x/\text{SiN}_x$  ARC on the front surface of the N-type TOPCon solar cell was changed to  $\text{AlO}_x/\text{SiN}_x/\text{SiO}_x$  and  $\text{AlO}_x/\text{SiN}_x/\text{SiO}_x\text{N}_y/\text{SiO}_x$  ARCs. By adjusting the thickness of each layer and studying the optical reflectivity, transmitted photon flux density and electrical properties of different layer combinations in the experiment, the best thickness combination for multilayer antireflection coating was finally obtained.

## 2. Materials and experiments

The N-type (phosphor-doped) Czochralski silicon wafers with a resistivity of  $0.4\text{--}1.6 \Omega \cdot \text{cm}$  and thickness of  $130 \pm 10 \mu\text{m}$  were used in this paper. The silicon wafers were cut into squares of  $182 \times 182 \text{ mm}^2$ , with a diagonal diameter of 247 mm after cutting the chamfers. The fabrication process of TOPCon solar cells in the experiments was shown in Fig. 1. Initially, the silicon wafers underwent cleaning and texturing in a NaOH solution and then cleaned with an HCl/HF solution to remove surface mechanical damage and metal impurities. To form a PN junction [23,24], the emitters were doped with  $\text{BCl}_3$  in a quartz furnace tube at  $1050 \pm 5 \text{ }^\circ\text{C}$  for 90 min, and the front sheet resistance was  $135 \pm 5 \text{ ohm/sq}$ . after doping. Then, the PN junction on the rear and edge was etched away with a NaOH solution. Subsequently, an ultra-thin oxide layer ( $2.0 \pm 0.2 \text{ nm}$ ) was deposited by the plasma-enhanced atomic layer deposition (PEALD) device using the silicon source (Bis (diethylamino) silane) at a flow rate of 2400 ml/min and the  $\text{O}_2$  at a flow rate of 3400 ml/min for 4-cycle at  $230 \pm 5 \text{ }^\circ\text{C}$ . Next, a phosphorus-doped amorphous silicon layer ( $85 \pm 5 \text{ nm}$ ) was deposited by

PECVD using  $\text{PH}_3$  (concentration of 4%) at a flow rate of 1100 ml/min and  $\text{SiH}_4$  at a flow rate of 2000 ml/min at  $415 \pm 5 \text{ }^\circ\text{C}$  for 920 s. Then, the rear amorphous silicon was converted into polycrystalline silicon (poly-Si) [25] through annealing in a tube furnace at  $900 \pm 5 \text{ }^\circ\text{C}$  for 40 min, and the rear sheet resistance was about  $45 \pm 5 \text{ ohm/sq}$ . Because there may be gaps between the wafers and the wafer carriers in the PECVD equipment, a thin poly-Si layer will be deposited at the edge on the front side during poly-Si deposition. Therefore, it was necessary to remove it through RCA cleaning and KOH alkaline etching after annealing. Subsequently, both the front borosilicate glass and the rear phosphosilicate glass were removed using HF. After the cleaning, the passivation and antireflection layer were deposited on the front and rear of the cells. Then, screen printing and firing were carried out to form a good ohmic contact of the cells. The temperature in the firing process can reach  $820 \text{ }^\circ\text{C}$ . After the above process, the cells were finally processed by photon injection hydrogenation to complete the manufacturing.

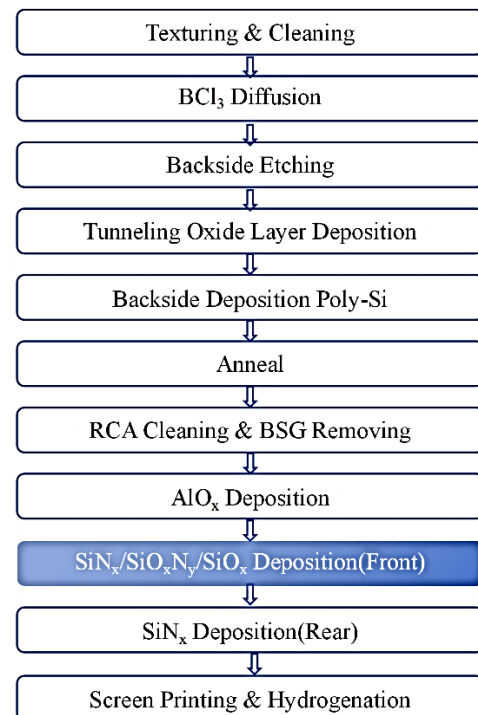


Fig. 1. The production process of solar cells in the experiment (colour online)

In the previous reports, researchers have explored several methods for the deposition of antireflection coatings, such as the atomic layer deposition (ALD) [26-28] and the PECVD technique [10,29]. In this paper, the deposition of ARCs was divided into three schemes, as shown in Fig. 2: (i)  $\text{AlO}_x/\text{SiN}_x$  ARC — a  $4.5 \pm 0.5 \text{ nm}$   $\text{AlO}_x$  film was deposited by atomic layer deposition (ALD) technique with trimethylaluminium and  $\text{H}_2\text{O}$  at  $400 \pm 5 \text{ }^\circ\text{C}$ , and then an  $80 \pm 5 \text{ nm}$   $\text{SiN}_x$  film was deposited by PECVD with  $\text{SiH}_4$  and

$\text{NH}_3$  at  $510 \pm 5$  °C; (ii)  $\text{AlO}_x/\text{SiN}_x/\text{SiO}_x$  ARC —  $\text{AlO}_x$  was deposited with the same thickness and deposition method as (i), then PECVD equipment was used to deposit  $\text{SiN}_x$  and  $\text{SiO}_x$  at  $510 \pm 5$  °C,  $\text{SiN}_x$  was first deposited by  $\text{SiH}_4$  and  $\text{NH}_3$ , and then  $\text{SiO}_x$  was deposited by  $\text{SiH}_4$  and  $\text{N}_2\text{O}$ ; (iii)  $\text{AlO}_x/\text{SiN}_x/\text{SiO}_x\text{N}_y/\text{SiO}_x$  ARC —  $\text{AlO}_x$  was deposited with

the same thickness and deposition method as (i), then PECVD equipment was used to deposit  $\text{SiN}_x$ ,  $\text{SiO}_x\text{N}_y$  and  $\text{SiO}_x$  at  $510 \pm 5$  °C,  $\text{SiN}_x$  was first deposited by  $\text{SiH}_4$  and  $\text{NH}_3$ , then  $\text{SiO}_x\text{N}_y$  was deposited by  $\text{SiH}_4$ ,  $\text{NH}_3$  and  $\text{N}_2\text{O}$ , and  $\text{SiO}_x$  was finally deposited by  $\text{SiH}_4$  and  $\text{N}_2\text{O}$ .

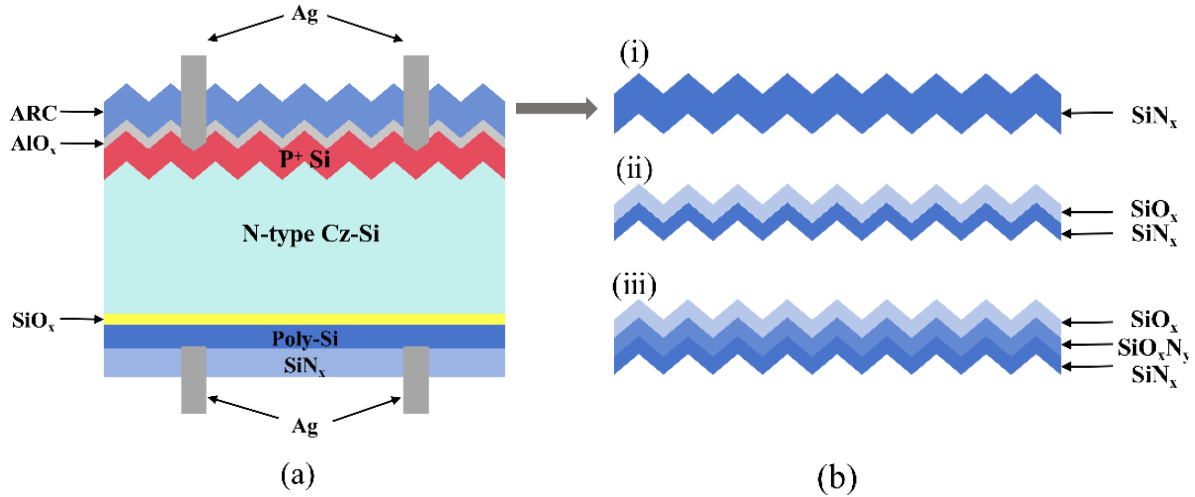


Fig. 2. (a) Structure diagram of N-type TOPCon solar cell; (b) Three ARC schemes:  $\text{SiN}_x$ ,  $\text{SiN}_x/\text{SiO}_x$ ,  $\text{SiN}_x/\text{SiO}_x\text{N}_y/\text{SiO}_x$  (colour online)

The three ARCs deposition conditions are shown in Table 1.

Table 1. Three ARCs deposition conditions

	ARCs	$\text{SiH}_4$ (sccm)	$\text{NH}_3$ (sccm)	$\text{N}_2\text{O}$ (sccm)	time (s)	temperature (°C)	power (W)	pressure (Pa)
i	$\text{SiN}_x$	1044	9169	0	800	510	11000	220
ii	$\text{SiN}_x$	1044	9169	0	400	510	11000	220
	$\text{SiO}_x$	500	0	9545	400		9000	120
iii	$\text{SiN}_x$	1044	9169	0	300	510	11000	220
	$\text{SiO}_x\text{N}_y$	860	1320	6435	200		9000	120
	$\text{SiO}_x$	500	0	9545	300		9000	120

The refractive indices of  $\text{SiN}_x$ ,  $\text{SiO}_x\text{N}_y$  and  $\text{SiO}_x$  film in this paper were respectively 2.05, 1.85 and 1.55. The film thickness was adjusted by controlling the reaction time to seek the optimal combination of the film thickness. The film thickness and refractive index were measured by Spectroscopic ellipsometry. After the deposition of the films, the electrical properties of the cells were tested under the irradiation conditions simulated AM1.5G, 1000  $\text{W}/\text{m}^2$  and 25°C.

### 3. Results and discussion

#### 3.1. Comparison and analysis of optical reflectivity of the cells

The deposition of the ARC on the front surface of N-type TOPCon solar cells was an effective way to improve the power conversion efficiency. To explore the antireflection effect of different coatings, three ARCs with different structures were deposited on the front surface of TOPCon solar cells. Due to the requirement for the passivation of the  $\text{P}^+$  emitter, a 4.5 nm  $\text{AlO}_x$  was fixed as the innermost layer in the experiments.

The three different coating stacks were  $\text{AlO}_x/\text{SiN}_x$  (80 nm),  $\text{AlO}_x/\text{SiN}_x$ (40 nm)/ $\text{SiO}_x$ (40 nm) and  $\text{AlO}_x/\text{SiN}_x$ (30 nm)/ $\text{SiO}_x\text{N}_y$ (20 nm)/ $\text{SiO}_x$ (30 nm).

The optical reflectivity curves of the solar cells with different ARCs were measured and shown in Fig. 3.

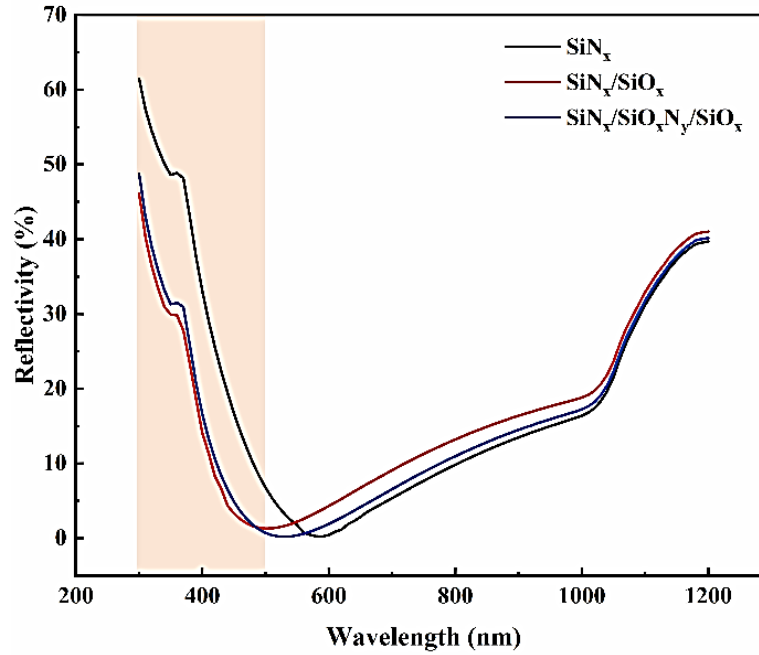


Fig. 3. Optical reflectivity curves of the cells with different ARCs (colour online)

For a more intuitive comparison of the optical reflectivity of different ARCs, the average optical reflectivity was calculated from Eq. (1) according to the optical reflectivity curves in Fig. 1. The results were presented in Table 2.

$$\bar{R} = \frac{1}{\lambda_2 - \lambda_1} \int_{\lambda_1}^{\lambda_2} R(\lambda) d(\lambda) \quad (2)$$

Table 2. Average optical reflectivity of the cells with different ARCs

ARC	$\text{AlO}_x/\text{SiN}_x$	$\text{AlO}_x/\text{SiN}_x/\text{SiO}_x$	$\text{AlO}_x/\text{SiN}_x/\text{SiO}_x\text{N}_y/\text{SiO}_x$
Average optical reflectivity (%)	18.34	16.73	15.70

From Fig. 3, the optical reflectivity of the  $\text{AlO}_x/\text{SiN}_x$  stack was much higher than that of the  $\text{AlO}_x/\text{SiN}_x/\text{SiO}_x$  stack and  $\text{AlO}_x/\text{SiN}_x/\text{SiO}_x\text{N}_y/\text{SiO}_x$  stack at a wavelength of 300~500 nm [5]. The reason is that  $\text{SiN}_x$  hardly achieve an excellent antireflection effect in a wide spectrum. Therefore, the solar cell had a high optical reflectivity when  $\text{SiN}_x$  was used as the outermost antireflection layer.

According to the optical reflection theory, the optimum refractive index of the front reflective film was [19],

$$n = \sqrt{n_0 n_{Si}} \quad (2)$$

where  $n$  is the refractive index of the optimum antireflection film,  $n_0$  is the air refractive index, and  $n_{Si}$  is the bare silicon refractive index.  $n_0=1.00$ ,  $n_{Si}=3.42$ , and then  $n=1.85$  can be obtained.

The refractive index of  $\text{SiN}_x$  was regulated within the

range of 1.90 ~ 2.70 [5]. A reduction in the refractive index of  $\text{SiN}_x$  will have an impact on densification, which in turn affects the passivation effect and the potential induced degradation (PID) blocking effect [5]. So, the refractive index of  $\text{SiN}_x$  was usually used above 2 in PV industry. When  $\text{SiN}_x$  was used as an antireflection film, the refractive index was different from the required refractive index  $n$ , which could not perfectly meet the requirements of an antireflection film.

Fortunately, the comprehensive refractive index of the front antireflection stack can be effectively adjusted by introducing a  $\text{SiO}_x$  film with a low refractive index. However, there is a certain refractive index difference between  $\text{SiO}_x$  and  $\text{SiN}_x$ . The greater the refractive index difference between the two layers, the greater the optical reflectance at their interface is likely to be. Therefore, when  $\text{AlO}_x/\text{SiN}_x/\text{SiO}_x$  was used as the antireflection stack, there was still a large space for reducing the optical reflectivity, and it was suitable to introduce the  $\text{SiO}_x\text{N}_y$  transitional layer

between  $\text{SiN}_x$  and  $\text{SiO}_x$ , since the refractive index of  $\text{SiO}_x\text{N}_y$  can be controlled between 1.45~1.90 by adjusting the process parameters [30]. Moreover, the refractive index matching multilayer structure exhibited a wider spectral response, which was more conducive to improving the antireflection effect and power conversion efficiency of the cell. It can be observed from Tab. 1 that the optical reflectivity of the cells with different ARCs was found to be in the order  $\text{AlO}_x/\text{SiN}_x > \text{AlO}_x/\text{SiN}_x/\text{SiO}_x > \text{AlO}_x/\text{SiN}_x/\text{SiO}_x\text{N}_y/\text{SiO}_x$ , thus

confirming that the introduction of  $\text{SiO}_x$  and  $\text{SiO}_x\text{N}_y$  layers was indeed conducive to reducing the optical reflectivity of multilayer films.

To verify the impact of multilayer ARC on the power conversion efficiency of solar cells, the electrical properties of TOPCon solar cells with  $\text{AlO}_x/\text{SiN}_x$ ,  $\text{AlO}_x/\text{SiN}_x/\text{SiO}_x$  and  $\text{AlO}_x/\text{SiN}_x/\text{SiO}_x\text{N}_y/\text{SiO}_x$  ARCs were measured under the irradiation conditions simulated AM1.5G, 1000 W/m<sup>2</sup> and 25°C. The results are illustrated in Fig. 4.

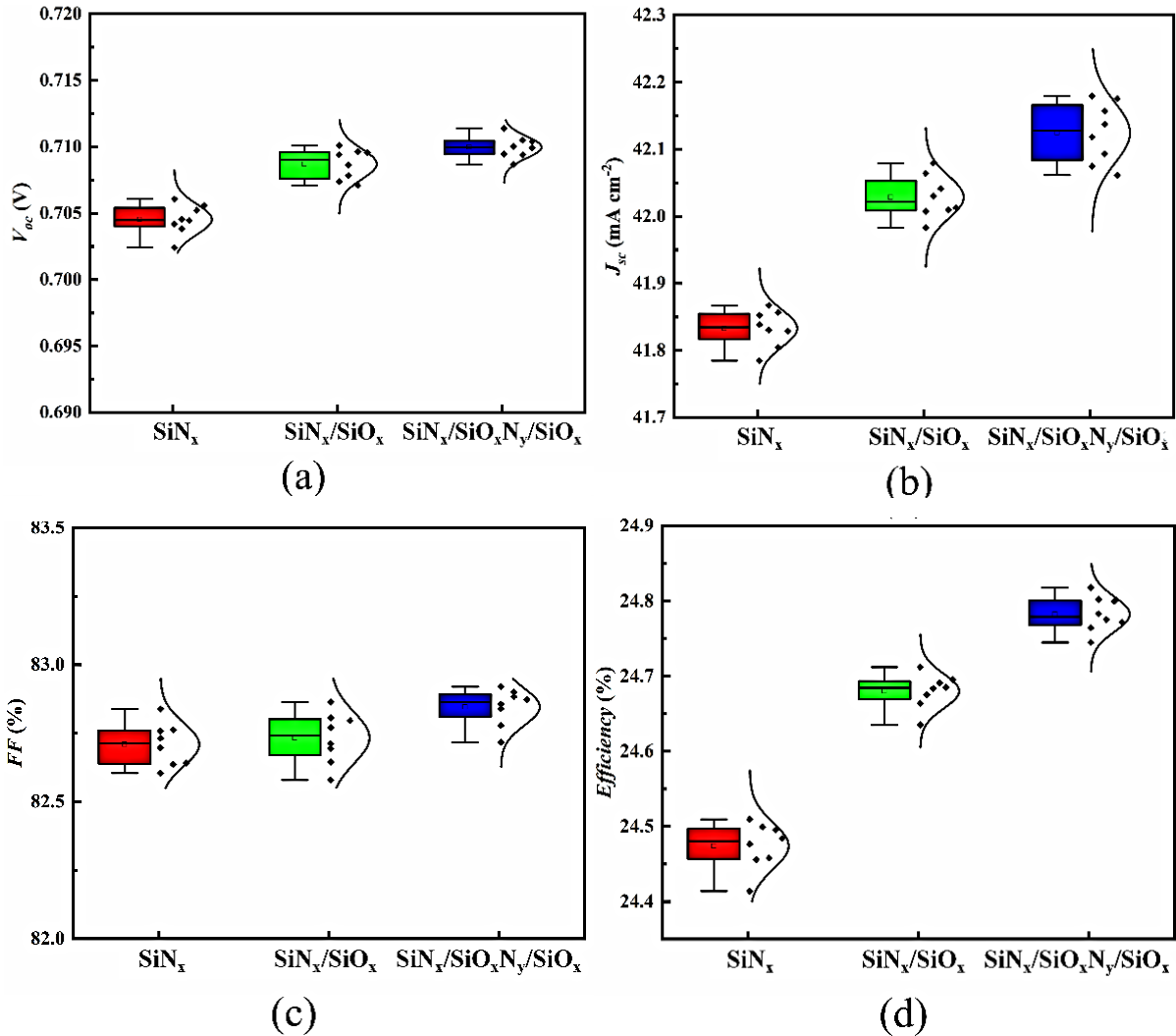


Fig. 4 Electrical performances of the solar cells with different ARCs (a) open-circuit voltage; (b) short-circuit current density; (c) Fill factor; (d) Power conversion efficiency (colour online)

As shown in Fig. 4, among the solar cells with  $\text{AlO}_x/\text{SiN}_x$ ,  $\text{AlO}_x/\text{SiN}_x/\text{SiO}_x\text{N}_y/\text{SiO}_x$  and  $\text{AlO}_x/\text{SiN}_x/\text{SiO}_x\text{N}_y/\text{SiO}_x$  ARCs, the cells with  $\text{AlO}_x/\text{SiN}_x/\text{SiO}_x\text{N}_y/\text{SiO}_x$  ARC stack had the best electrical performances. This was mainly because the films at the front-end with lower optical reflectivity led to an enhancement in the short-circuit current density ( $J_{sc}$ ) of the cells.

Compared with the cells with  $\text{AlO}_x/\text{SiN}_x$  stack, the average  $J_{sc}$  of the cells with  $\text{AlO}_x/\text{SiN}_x/\text{SiO}_x$  ARC increased by 195  $\mu\text{A cm}^{-2}$ , and the cells with  $\text{AlO}_x/\text{SiN}_x/\text{SiO}_x\text{N}_y/\text{SiO}_x$  ARC increased by 290  $\mu\text{A cm}^{-2}$ . This gain was mainly due to the optical reflectivity reducing of the cells as shown in

Fig. 3 and Table 1. Meanwhile, the thickness decreases of  $\text{SiN}_x$  and the combination of  $\text{SiN}_x$  with  $\text{SiO}_x$  and  $\text{SiO}_x\text{N}_y$  effectively reduced the light absorption at the short-wavelength range, since  $\text{SiN}_x$  has a high light absorption in 300-500 nm [5]. The introduction of  $\text{SiO}_x\text{N}_y$  between  $\text{SiN}_x$  and  $\text{SiO}_x$  also made the refractive index difference between the  $\text{SiN}_x$  and  $\text{SiO}_x$  layers smaller, thus reducing the optical reflectivity, and causing a 95  $\mu\text{A cm}^{-2}$  increase in  $J_{sc}$  compared between the cells with  $\text{AlO}_x/\text{SiN}_x/\text{SiO}_x\text{N}_y/\text{SiO}_x$  and  $\text{AlO}_x/\text{SiN}_x/\text{SiO}_x$  ARC stacks. Additionally, the introduction of  $\text{SiO}_x$  and  $\text{SiO}_x\text{N}_y$  films was more conducive to the glass powder in the Ag paste penetrating the dielectric

layer, forming better electrode contact. Thus, the open-circuit voltage ( $V_{oc}$ ) and fill factor ( $FF$ ) of solar cells with  $\text{AlO}_x/\text{SiN}_x/\text{SiO}_x$  ARC were also improved.

In summary, compared with the cells with  $\text{AlO}_x/\text{SiN}_x$  stack, the average power conversion efficiency of the solar cells with  $\text{AlO}_x/\text{SiN}_x/\text{SiO}_x$  ARC increased by 0.2% abs., and the average power conversion efficiency of the cells with  $\text{AlO}_x/\text{SiN}_x/\text{SiO}_x\text{N}_y/\text{SiO}_x$  ARC increased by 0.3% abs. The improvement in the efficiency of TOPCon solar cells was mainly due to the improvement of the short-circuit current density after the optimization of ARC. This result fully proved that the optimized  $\text{AlO}_x/\text{SiN}_x/\text{SiO}_x\text{N}_y/\text{SiO}_x$  ARC stack can achieve the purpose of reducing optical reflectivity and improving the power conversion efficiency of solar cells.

### 3.2. Optimization of $\text{SiN}_x/\text{SiO}_x\text{N}_y/\text{SiO}_x$ ARC thickness

The structure of the ARC on the front surface of the solar cells was critically important, as well as the thickness of each layer, which had a significant impact on the optical reflectivity of the solar cell. To further optimize the effect of ARC, the  $\text{SiN}_x/\text{SiO}_x\text{N}_y/\text{SiO}_x$  stack was optimized by adjusting the thickness of  $\text{SiN}_x$ ,  $\text{SiO}_x\text{N}_y$  and  $\text{SiO}_x$ . In the experiments,  $\text{SiN}_x(30 \text{ nm})/\text{SiO}_x\text{N}_y(20 \text{ nm})/\text{SiO}_x(30 \text{ nm})$  was used as the control group (Baseline), and the thickness was adjusted by controlling the deposition time. Since the films had different light absorption at different wavelengths, the optical reflectivity curves of the  $\text{AlO}_x/\text{SiN}_x/\text{SiO}_x\text{N}_y/\text{SiO}_x$  ARCs with various thicknesses were measured in this paper and their average optical reflectivity was calculated. The results are shown in Fig. 5.

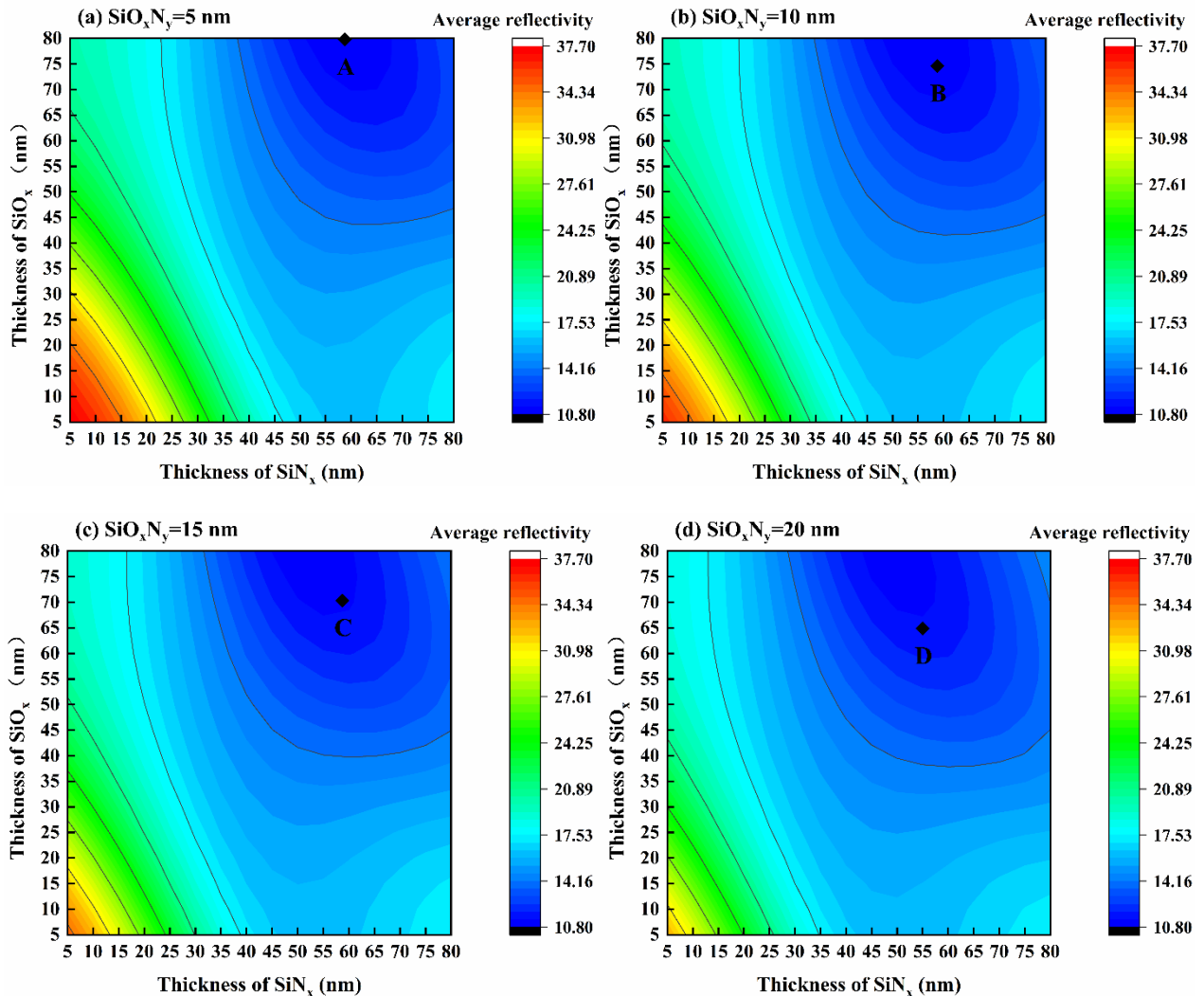


Fig. 5. Average optical reflectivity of the solar cells with  $\text{SiN}_x/\text{SiO}_x\text{N}_y/\text{SiO}_x$  ARCs in different thicknesses (a) The thickness of  $\text{SiO}_x\text{N}_y$  was 5 nm; (b) The thickness of  $\text{SiO}_x\text{N}_y$  was 10 nm; (c) The thickness of  $\text{SiO}_x\text{N}_y$  was 15 nm; (d) The thickness of  $\text{SiO}_x\text{N}_y$  was 20 nm (colour online)

Table 3. Optical reflectivity and film thickness of the points A, B, C and D

The lowest optical reflectivity point		A	B	C	D
Reflectivity Data (%)		10.83	10.82	10.92	11.00
Corresponding thickness of each layer in the ARC stack	SiN <sub>x</sub> (nm)	60	60	60	55
	SiO <sub>x</sub> N <sub>y</sub> (nm)	5	10	15	20
	SiO <sub>x</sub> (nm)	80	75	70	65

It was illustrated in Fig. 5 that the optical reflectivity varied with the thickness of ARC. And it can be seen from Table 3 that in the AlO<sub>x</sub>/SiN<sub>x</sub>/SiO<sub>x</sub>N<sub>y</sub>/SiO<sub>x</sub> ARC stack, when the thickness of SiO<sub>x</sub>N<sub>y</sub> was 10 nm, the lowest optical reflectivity was 10.82%, and the corresponding thickness of SiN<sub>x</sub> and SiO<sub>x</sub> was 60 nm 75 nm, respectively.

The ARCs thickness with the lowest reflectivity was obtained from the above experiments, however, solar cells work under the sunlight. The energy distribution of the AM1.5G solar spectrum is not uniform, and it is also inconsistent with the spectral response of the crystalline silicon solar cells. The optical reflectivity curves of the films also change the light energy distribution transmitted through the ARC. Therefore, the lowest simple average optical reflectivity did not mean the highest photon flux density obtained by crystalline silicon under sunlight. The ultimate consideration should maximum the total number of photons in the unit area and unit time, which transmitted through the medium layers to the surface of the silicon wafer in the response range of crystalline silicon, that was, the maximum photon flux density on the surface of the silicon wafer, as shown in Eq. (3):

$$N = \int_{\lambda_1}^{\lambda_2} \varphi(\lambda)(1-R(\lambda))d(\lambda) \quad (3)$$

where  $N$  represents the transmitted photon flux density,  $\lambda_1$  is 300 nm,  $\lambda_2$  is 1200 nm, 300~1200 nm is the response range of crystalline silicon solar cells,  $\varphi(\lambda)$  is the photon flux density of AM1.5G,  $R(\lambda)$  is the optical reflectivity of the ARCs.

The transmitted photon flux density of different ARCs was calculated by Eq. (3), and the results were shown in Fig. 6.

The transmitted photon flux density of ARCs with different thicknesses under the sunlight was different, and it was effectively enhanced by adjusting the film thickness. As shown in Tab. 4, when the thickness of SiO<sub>x</sub>N<sub>y</sub>, SiN<sub>x</sub> and SiO<sub>x</sub> was 10 nm, 55 nm and 65 nm respectively, the transmitted photon flux density was the maximum, as shown in Fig. 6.

To verify whether the power conversion efficiency of the cells increased when the transmitted photon flux density reached the maximum, the electrical performances of the cells with different ARC thicknesses on the points of E, F, G and H were measured under the irradiation conditions simulated AM1.5G, 1000 W/m<sup>2</sup> and 25°C. The results compared with the Baseline conditions were shown in Table 5.

However, Table 5 showed that when the transmitted photon flux density reached the maximum, the efficiency of the solar cell did not increase but had a significant decline. Compared with the Baseline, the main decreases in the performances were the  $V_{oc}$  and  $FF$ . It can be seen that when the transmitted photon flux density reached the maximum, the total thickness of AlO<sub>x</sub>/SiN<sub>x</sub>/SiO<sub>x</sub>N<sub>y</sub>/SiO<sub>x</sub> ARCs reached 130~140 nm. When the front surface ARC stack of the solar cells was too thick, it had a significant impact on the subsequent metallization process so that the Ag paste could not penetrate to the surface of the silicon in the firing process to form an excellent ohmic contact with the P<sup>+</sup> emitter, thus significantly reducing the  $V_{oc}$  and  $FF$ .

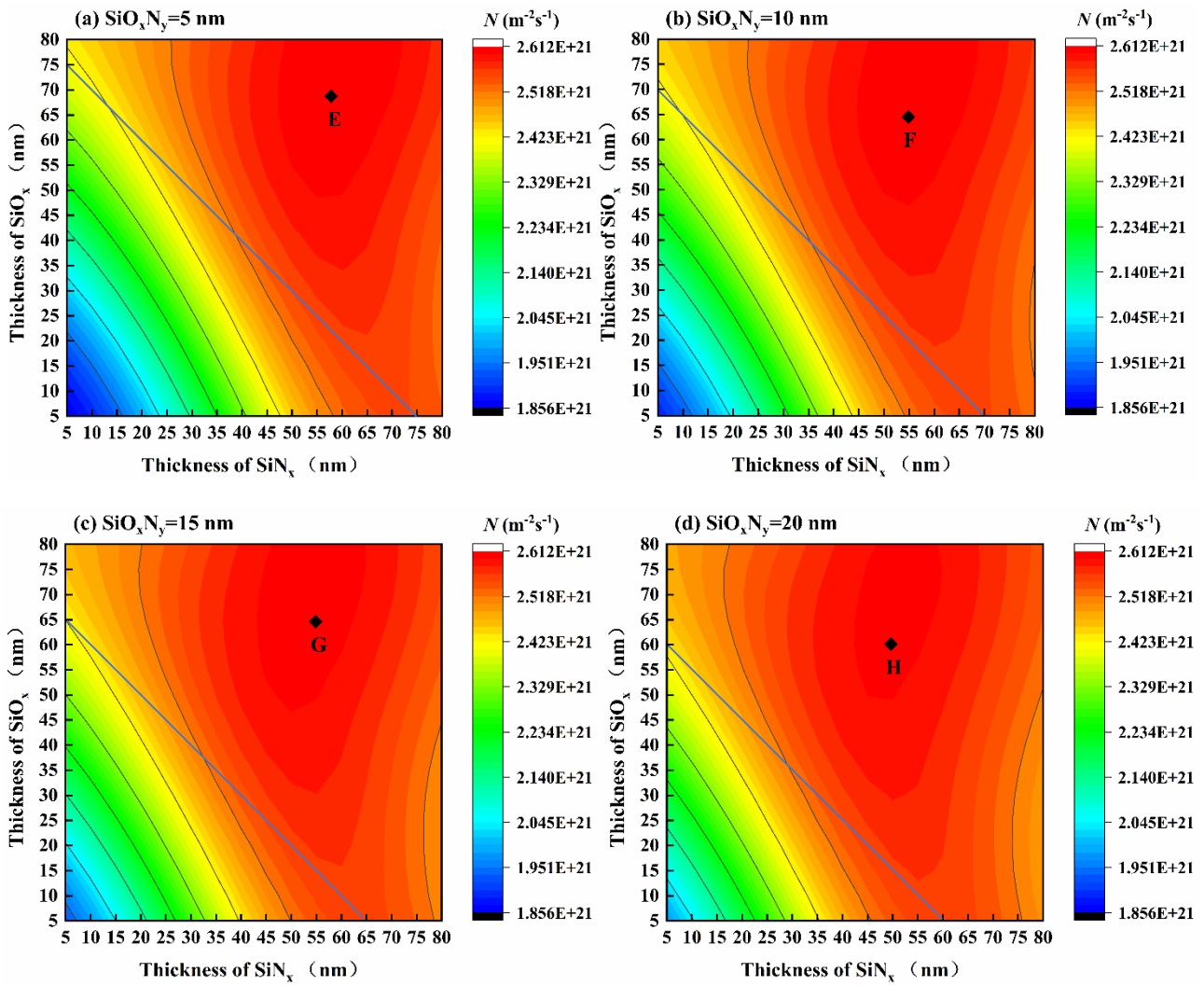


Fig. 6.  $N$  of the solar cells with  $\text{SiN}_x/\text{SiO}_x\text{N}_y/\text{SiO}_x$  ARCs in different thicknesses (a) The thickness of  $\text{SiO}_x\text{N}_y$  was 5 nm; (b) The thickness of  $\text{SiO}_x\text{N}_y$  was 10 nm; (c) The thickness of  $\text{SiO}_x\text{N}_y$  was 15 nm; (d) The thickness of  $\text{SiO}_x\text{N}_y$  was 20 nm (colour online)

Table 4.  $N$  and film thickness of the points E, F, G and H

The maximum $N$ point		E	F	G	H
$N (\times 10^{21} \text{ m}^{-2} \text{ s}^{-1})$		2.609	2.611	2.606	2.602
Corresponding thickness of each layer in the ARC stack	$\text{SiN}_x (\text{nm})$	60	55	55	50
	$\text{SiO}_x\text{N}_y (\text{nm})$	5	10	15	20
	$\text{SiO}_x (\text{nm})$	70	65	65	60

Table 5. Electric performance of solar cells under E, F, G, H and Baseline conditions (Average of 200 samples per group)

	$V_{oc} (\pm 0.0005 \text{ V})$	$J_{sc} (\pm 0.06 \text{ mA cm}^{-2})$	$FF (\pm 0.2 \%)$	$\text{Efficiency} (\pm 0.05 \%)$
Baseline	0.7100	42.12	82.8	24.78
E	0.6957	42.09	81.6	23.96
F	0.6969	42.10	81.8	24.04
G	0.6956	42.06	81.2	23.85
H	0.6954	42.06	81.1	23.78

The influence of the pool ohmic contact can be observed from the electroluminescence (EL) test, as shown in Fig. 7. EL is a kind of radiation recombination by applying voltage at both ends of the electrode to make the solar cell pass through, and inject carriers in the area without defects. If the EL is black, it may be due to the obstruction of carrier injection in some areas due to the contact problem, and fewer carriers are obtained in this area

of the solar cell, so that the cell emits less light, and the EL is black. Therefore, Fig. 7 can reflect the contact problem through EL diagram. The EL figures were substantially darker than that of the cells under the Baseline conditions. The results demonstrated that Ag paste did not perfectly penetrate the antireflection layer during the firing process, resulting in a more significant impact on the  $V_{oc}$  and  $FF$ , which reduced the efficiency of the solar cell.

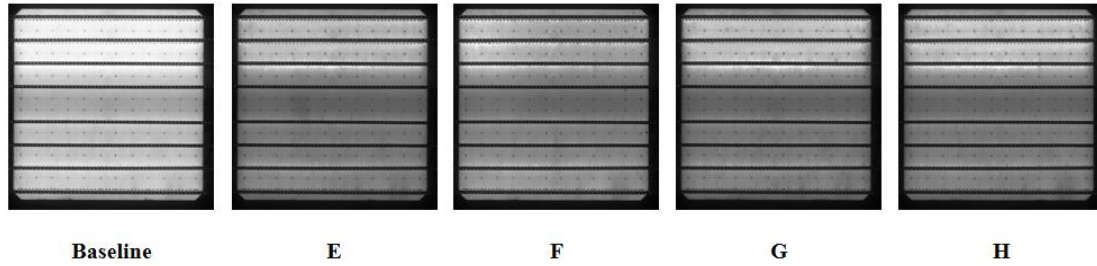


Fig. 7. EL figures of solar cells with different ARCs thicknesses

To ensure the contact characteristics of metal fingers in the subsequent process of the cell preparation, the total thickness of the  $\text{SiN}_x/\text{SiO}_x\text{N}_y/\text{SiO}_x$  stack was fixed around 85 nm (the blue line in Fig. 6), the EL figure of solar cells was relatively bright, and Ag paste could penetrate the antireflection layer and formed good contact with the  $\text{P}^+$  emitter during the metallization. In other words, in order to ensure excellent electrode contact, the maximum

transmitted photon flux density should be searched on the blue line in Fig. 6. In the following experiments, a certain number of ARC stacks with different thicknesses were respectively taken on the blue line in Fig. 6 to prepare the cells, and the electrical performances of the solar cells were measured under the irradiation conditions simulated AM1.5G, 1000  $\text{W}/\text{m}^2$  and 25°C, as shown in Table 6.

Table 6. Electrical properties and transmitted photon flux density of solar cells with total thickness at 85 nm (Average of 200 samples per group)

Thickness of $\text{SiO}_x\text{N}_y$ (nm)	Thickness of $\text{SiN}_x$ (nm)	Thickness of $\text{SiO}_x$ (nm)	$V_{oc}$ ( $\pm 0.0005$ V)	$J_{sc}$ ( $\pm 0.06$ mA $\text{cm}^{-2}$ )	$FF$ ( $\pm 0.2$ %)	Efficiency ( $\pm 0.05$ %)	$N$ ( $\times 10^{21}$ $\text{m}^{-2}\text{s}^{-1}$ )
5	50	30	0.706	41.95	82.6	24.52	2.550
	55	25	0.707	42.06	82.8	24.60	2.557
	60	20	0.709	42.14	82.9	<b>24.70</b>	<b>2.559</b>
	65	15	0.708	42.09	82.8	24.62	2.558
	70	10	0.706	42.01	82.7	24.57	2.554
10	50	25	0.707	42.01	82.8	24.58	2.554
	55	20	0.709	42.11	82.9	24.68	2.559
	60	15	0.710	42.21	83.0	<b>24.84</b>	<b>2.561</b>
	65	10	0.708	42.08	82.8	24.61	2.557
	70	5	0.706	41.99	82.7	24.56	2.551
15	45	25	0.706	42.01	82.7	24.56	2.552
	50	20	0.708	42.10	82.8	24.65	2.558
	55	15	0.710	42.15	83.0	<b>24.79</b>	<b>2.560</b>
	60	10	0.709	42.14	82.9	24.72	2.559
	65	5	0.707	42.02	82.8	24.58	2.555
20	40	25	0.706	41.94	82.6	24.51	2.548
	45	20	0.707	42.05	82.8	24.59	2.556
	50	15	0.709	42.15	83.0	24.75	2.559
	55	10	0.710	42.15	83.0	<b>24.77</b>	<b>2.560</b>
	60	5	0.709	42.13	82.9	24.69	2.559

It can be seen from Table 6, when the fixed total thickness was 85 nm and the influence of metallization on solar cell contact was excluded, the changing trend of solar cell efficiency was agreed with that of the transmitted photon flux density on the blue line in Fig. 6. With the increase of the transmitted photon flux density, the short-circuit current density increased and the efficiency increased gradually. Finally, it was determined that when the ARC stack was  $\text{SiN}_x(60 \text{ nm})/\text{SiO}_x\text{N}_y(10 \text{ nm})/\text{SiO}_x(15 \text{ nm})$ , the transmitted photon flux density reached the maximum value, and the efficiency also reached the maximum value of 24.84% at this time.

#### 4. Conclusion

In this paper, the front surface antireflection layer of the TOPCon solar cells was optimized. The  $\text{AlO}_x/\text{SiN}_x/\text{SiO}_x$  multilayer ARC stack and  $\text{AlO}_x/\text{SiN}_x/\text{SiO}_x\text{N}_y/\text{SiO}_x$  multilayer ARC stack were designed to replace the traditional  $\text{AlO}_x/\text{SiN}_x$  stack on the front surface of the N-type TOPCon solar cells. The  $\text{AlO}_x/\text{SiN}_x/\text{SiO}_x$  and  $\text{AlO}_x/\text{SiN}_x/\text{SiO}_x\text{N}_y/\text{SiO}_x$  ARCs effectively reduced the optical reflectivity of the solar cell surface to the incident light and improved the short wavelength light absorption. Compared with the traditional solar cells with  $\text{AlO}_x/\text{SiN}_x$  stack, the efficiency of the solar cells with  $\text{AlO}_x/\text{SiN}_x/\text{SiO}_x$  ARC reached 24.68%, and the efficiency of the solar cells with  $\text{AlO}_x/\text{SiN}_x/\text{SiO}_x\text{N}_y/\text{SiO}_x$  ARC reached 24.78%, respectively higher than the former 0.2%<sub>abs.</sub> and 0.3%<sub>abs.</sub> The improvement in power conversion efficiency was mainly due to the reduction of the surface optical reflectivity, which increased the output current density. The experimental results showed that it was feasible to use  $\text{AlO}_x/\text{SiN}_x/\text{SiO}_x$  and  $\text{AlO}_x/\text{SiN}_x/\text{SiO}_x\text{N}_y/\text{SiO}_x$  instead of  $\text{AlO}_x/\text{SiN}_x/\text{SiO}_x$  ARC, in which  $\text{AlO}_x/\text{SiN}_x/\text{SiO}_x\text{N}_y/\text{SiO}_x$  ARC was more conducive to reducing the surface optical reflectivity, so as to improve the electrical performances of solar cells.

In addition, this paper further optimized the thickness of each film in the  $\text{SiN}_x/\text{SiO}_x\text{N}_y/\text{SiO}_x$  ARC stack. Through the comparative analysis of the optical reflectivity, the concept of transmitted photon flux density was proposed, and the contact characteristics between electrode and Si during the metallization were taken into account. It was finally obtained that when the thickness of  $\text{SiN}_x$ ,  $\text{SiO}_x\text{N}_y$  and  $\text{SiO}_x$  was 60 nm, 10 nm and 15 nm, the efficiency of the TOPCon solar cell reached a maximum of 24.84%. The structure and optimal thickness combination of the TOPCon solar cell front surface antireflection coating were further determined.

ARCs were deposited by PECVD equipment, which can effectively improve efficiency at a low-cost increase. Subsequently, the stability under temperature cycle or ultraviolet irradiation can be tested to further explore the effectiveness of ARCs.

#### Author contributions

MEILING ZHANG: Writing – original draft, Data curation, Methodology; MEILIN PENG: Investigation, Formal analysis; QIQI WANG: Investigation, Formal analysis; XI XI: Project guidance, Writing – review & editing, Resources; Conceptualization; GUILIN LIU: Writing - review & editing. JIANBO SHAO: Investigation, Resources.

#### Funding

This research was supported by the National Natural Science Foundation of China (Grant No. 61804066), Jiangsu Funding Program for Excellent Postdoctoral Talent (2024ZB526).

#### Conflicts of interest

The authors declare no conflict of interest.

#### References

- [1] Z. J. Fang, G. T. Chen, Q. Ye, R. H. Qu, J. Chin. Lasers **36**, 5 (2009).
- [2] F. Feldmann, M. Bivour, C. Reichel, M. Hermle, S. W. Glunz, Sol. Energy Mater. Sol. Cells **120**, 270 (2014).
- [3] A. Moldovan, F. Feldmann, M. Zimmer, J. Rentsch, J. Benick, M. Hermle, Sol. Energy Mater. Sol. Cells **142**, 123 (2015).
- [4] H. Bencherif, L. Dehimi, F. Pezzimenti, F. G. Della Corte, Optik **182**, 682 (2019).
- [5] M. H. Elshorbagy, K. Abdel-Hady, H. Kamal, J. Alda, Opt. Commun. **390**, 130 (2017).
- [6] S. Park, H. Park, D. Kim, J. Nam, J. Yang, D. Lee, B. K. Min, K. N. Kim, S. J. Park, S. Kim, D. Suh, D. Kim, H. S. Lee, Y. Kang, Curr. Appl. Phys. **17**, 517 (2017).
- [7] M. Boulesbaa, Spectrosc. Lett. **50**, 5 (2017).
- [8] M. C. Wei, S. J. Chang, C. Y. Tsia, C. H. Liu, S. C. Chen, Sol. Energy **80**, 215 (2006).
- [9] W. D. Huang, X. H. Wang, M. Sheng, L. Q. Xu, F. Stubhan, L. Luo, T. Feng, X. Wang, F. M. Zhang, S. C. Zou, Mater. Sci. Eng. B-Adv. **98**, 248 (2003).
- [10] J. Kim, J. Hong, S. H. Lee, J. Korean Phys. Soc. **44**, 479 (2004).
- [11] J. Benick, B. Hoex, M. C. M. van de Sanden, W. M. M. Kessels, O. Schultz, S. W. Glunz, Appl. Phys. Lett. **92**, 25 (2008).
- [12] B. Hoex, J. Schmidt, P. Pohl, M. C. M. van de Sanden, W. M. M. Kessels, J. Appl. Phys. **104**, 4 (2008).
- [13] J. W. Lim, C. K. Jin, K. Y. Lim, Y. J. Lee, Nano Energy **33**, 12 (2017).
- [14] X. J. Ma, Z. H. Si, D. Yang, T. Lin, S. C. Feng, Laser Optoelectron. Prog. **55**, 6 (2018).

- [15] A. V. Timofeev, A. I. Mil'shtein, D. N. Grigorev, *Optoelectron. Instrum.* **59**, 612 (2023).
- [16] G. J. Hou, C. Sanchez-Perez, I. Rey-Stolle, *IEEE J. Photovolt.* **14**, 93 (2024).
- [17] G. C. Han, P. Luo, K. B. Li, Z. Y. Liu, Y. H. Wu, *Appl. Phys. A-Mater.* **74**, 243 (2002).
- [18] J. Ko, D. Gong, K. Pillai, K. S. Lee, M. Ju, P. Choi, K. R. Kim, J. Yi, B. Choi, *Thin Solid Films* **519**, 6887 (2011).
- [19] Q. Ma, W. J. Zhang, D. H. Ma, Z. Q. Fan, X. B. Ma, Z. Y. Jiang, *Optik* **177**, 123 (2019).
- [20] L. V. Mercaldo, I. Usatii, P. D. Veneri, *Energies* **9**, 218 (2016).
- [21] L. Remache, E. Fourmond, A. Mahdjoub, J. Dupuis, M. Lemiti, *Mater. Sci. Eng. B-Adv.* **176**, 45 (2011).
- [22] Y. J. Wang, X. L. Cheng, Z. L. Lin, C. S. Zhang, F. Zhang, *Vacuum* **72**, 345 (2003).
- [23] J. X. Ye, B. Ai, J. S. Jin, D. P. Qiu, R. X. Liang, H. Shen, *Int. J. Photoenergy* **2019**, 1 (2019).
- [24] P. Padhamnath, A. Khanna, N. Nandakumar, A. G. Aberle, S. Duttagupta, *Sol. Energy Mater. Sol. Cells* **230**, 111217 (2021).
- [25] Z. Zhang, M. D. Liao, Y. Q. Huang, X. Q. Guo, Q. Yang, Z. X. Wang, T. Gao, C. H. Shou, Y. H. Zeng, B. J. Yan, J. C. Ye, *Solar RRL* **3**, 10 (2019).
- [26] B. Hoex, S. B. S. Heil, E. Langereis, M. C. M. van de Sanden, W. M. M. Kessels, *Appl. Phys. Lett.* **89**, 4 (2006).
- [27] Z. Xin, Z. P. Ling, N. Nandakumar, G. Kaur, C. M. Ke, B. C. Liao, A. G. Aberle, R. Stangl, *Japanese Journal of Applied Physics* **56**, 8 (2017).
- [28] D. Li, T. Kunz, N. Wolf, J. P. Liebig, S. Wittmann, T. Ahmad, M. T. Hessmann, R. Auer, M. Göken, C. J. Brabec, *Thin Solid Films* **583**, 25 (2015).
- [29] X. S. Wu, Z. F. Zhang, Y. Liu, X. N. Chu, Y. P. Li, *Solar Energy* **111**, 277 (2015).
- [30] A. del Prado, E. San Andrés, F. L. Martinez, I. Mártil, G. González-Díaz, W. Bohne, J. Röhrich, B. Selle, M. Fernández, *Vacuum* **67**, 507 (2002).

---

\*Corresponding author: xi.xi@jiangnan.edu.cn